

Non-Hermiticity in quantum mechanics

Ana Fabela Hinojosa ¹

Supervisors:

Dr. Jesper Levinsen

Prof. Meera Parish

SCHOOL OF PHYSICS & ASTRONOMY



MONASH University

June 2021

¹acfab1@student.monash.edu.au

“It is not the strongest of the species that survives, not the most intelligent that survives. It is the one that is the most adaptable to change.”

Charles Darwin

Contents

1	Introduction	1
1.1	Good ol' quantum mechanics	1
1.2	Adopting a new assumption	1
1.3	PT -symmetric quantum mechanics	2
1.4	Nerd-Sniped	3
2	My aborted simulation	5
2.1	Methods	5
2.2	Results	6
3	Reproducing Bender's figure	7
3.1	Methods	7
3.1.1	WKB approximation	7
3.1.2	Matrix equations	8
3.2	Results	11
3.2.1	The region of unbroken PT -symmetry	11
3.2.2	The region of broken PT -symmetry	13
3.2.3	The behaviour of eigenstates	14
3.2.4	The full version of the figure	15
4	Discussion	16
4.1	Complex WKB	16
4.2	<i>Stokes wedges</i> and boundary conditions	16
4.3	PT -symmetry breaking	17
4.4	Exceptional points	18
5	Conclusion	20
6	Acknowledgements	21

List of Figures

- 1.1 If there are two subsystems, call them A and B, and both subsystems are in contact with the outside environment, where the set-up is that the subsystem A gains energy while subsystem B loses the same amount of energy. Then we can consider the A and B subsystems as time-reversed versions of each other. Taken together as a larger combined system, then the AB system has no net probability flux. Notice that when we exchange A for B there is no change to the composite system, This means that the combined AB system is PT -symmetric. 2
- 1.2 The relevant XKCD comic -Nerd Sniping- <https://xkcd.com/356/>. Illustrates what happened to me during my project. 3
- 1.3 This is Figure 1. in reference [3]. It exemplifies the behaviour of the eigenvalue spectra of the general parametric family of non-Hermitian Hamiltonians $\hat{H} = \hat{p}^2 + \hat{x}^2(i\hat{x})^\epsilon$ as a function of the real parameter ϵ . All the eigenvalues visible in this figure are real valued. The PT -symmetry breaks at the $\epsilon = 0$, which corresponds to the Hamiltonian for the classic one dimensional harmonic oscillator. When $\epsilon \geq 0$ the spectra are real, positive and discrete. Energy levels increase with increasing ϵ . In the region corresponding to $-1 \leq \epsilon \leq 0$ there is a finite number of real positive eigenvalues and an infinite number of complex-conjugate pairs of eigenvalues (not depicted). The number of real eigenvalues decreases as ϵ decreases from 0 to -1 , for ϵ that are more negative than the value $\epsilon = -0.57793$ the only remaining real eigenvalue corresponds to the ground-state energy. At the value $\epsilon = -1$ the spectrum is null, as all the eigenvalues diverge to infinity. 4

- 2.1 These are 6 frames of my simulation of a right propagating Gaussian wave packet in space as a function of time. The horizontal axes of every frame correspond to the spatial coordinate x (dimensionless) and the vertical axes of every frame correspond to the real and imaginary parts of the Gaussian wave packet. The earliest time frame is the top left panel, corresponding to wave packet at time $t = 15600$ as can be seen in that plot's title. The panels in this arrangement should be studied from left to right and top to bottom. An "undesirable" reflection of the real part of the wave packet at the boundary is visible specially in the last 3 frames from left to right, corresponding to times $t = 24000$, $t = 26800$ and $t = 29600$ as can be seen in the plots' titles from left to right respectively. . . . 6

- 3.1 From left to right the image is zoomed. Here I demonstrate that my WKB energy results (visible as the blue plot) for the case on the non-Hermitian, PT -symmetric Hamiltonian $\hat{H} = \hat{p}^2 + \hat{x}^2(i\hat{x})$ (ie. the case: $\epsilon = 1$) are in agreement with the energy values reported in Bender's work. Bender's results were obtained by the Runge-Kutta method (orange plot) and by the WKB approximation (green plot). All the energies (energy is the vertical axis) presented in this plot were obtained using $n \in [0, 9]$. n is visible as the horizontal axis for this plot. 11
- 3.2 My implementation of the WKB method on the family of non-Hermitian, PT -symmetric Hamiltonians $\hat{H} = \hat{p}^2 + \hat{x}^2(i\hat{x})^\epsilon$ for $\epsilon \geq 0$. My energy values (energy is the vertical axis) were in agreement with those visible in Figure 1.3 on page 4. All the energies presented in this plot are real valued, and they are bounded below by the eigenvalues corresponding to the ground-state visible here as a blue plot. The changing colours of every plot represent increasing values of n corresponding to the left hand side expression in the WKB quantisation condition: $(n + \frac{1}{2})\pi$. The horizontal axis is the range of values $0 \leq \epsilon \leq 3$. . . 12

- 3.3 This plot is an extension of Figure 1.3 on page 4. Here I display the discretised space of ϵ as 100 values in the horizontal axis, and the eigenvalues of the parametric family of PT -symmetric, non-hermitian Hamiltonians $\hat{H} = \hat{p}^2 + \hat{x}^2(i\hat{x})^\epsilon$ for the region corresponding to $\epsilon \leq 0$ in the vertical axis. This figure depicts fully real eigenvalues (black dots) and the points at which the eigenvalues become degenerate and then form complex-conjugate pairs. The real parts of these pairs of eigenvalues (blue dots) initially decrease as ϵ decreases but blow up suddenly as ϵ approaches -1. The imaginary parts of the eigenvalue pairs (red dots) remain finite and appear to decay to zero at $\epsilon = -1$ 13
- 3.4 These are 6 frames in the visualisation of the behaviour of the first and second excited states for the Hamiltonian in equation (3.1) in the region of broken PT -symmetry. The horizontal axes of each plot represent the x coordinate, and the vertical axes represent the wave functions. In addition to the legend I have added on the top left corner of each of the plots the corresponding eigenvalues to each of the wave functions, and the corresponding ϵ value to make note of this parametric dimension. On the top left panel, the ϵ value is most negative. The plots in this arrangement should be studied from left to right and top to bottom. Here I demonstrate how the structure of the eigenstates changes as we approach the ϵ value corresponding to the **exceptional point** (approximately $\epsilon = -0.576$). As ϵ varies, we can see the wave functions behave as mirror images of each other when the ϵ value is more negative than the exceptional point. Then at the approximate value of the exceptional point (visible in the top right plot), the wave functions overlap. As the ϵ values become less negative than the exceptional point, the states themselves become symmetric about zero. At the bottom right plot, we see that the states are the first and second excited states of the harmonic oscillator, ie. $\epsilon = 0$ 14
- 3.5 These are 6 frames in the visualisation of the behaviour of the probability density of the first and second excited states for the Hamiltonian in equation (3.1) in the region of broken PT -symmetry. Similarly to the previous figure, the horizontal axes of each plot represent the x coordinate, and the vertical axes represent the probability density of the states. In addition to the legend I have added on the top left corner of each of the plots the corresponding eigenvalues to each state, and the corresponding ϵ value to make note of this parametric dimension. On the top left panel, the ϵ value is most negative. The plots in this arrangement should be studied from left to right and top to bottom. Here I demonstrate how the eigenstates densities change as we approach the ϵ value corresponding to the **exceptional point** (approximately $\epsilon = -0.576$). As ϵ varies, we can see the densities behave as mirror images of each other when the ϵ value is more negative than the exceptional point. Then at the approximate value of the exceptional point (visible in the top right plot), the densities overlap. As the ϵ values become less negative than the exceptional point, the densities themselves become symmetric about zero. At the bottom right plot, we see that the states densities correspond to those of the first and second excited states of the harmonic oscillator, ie. $\epsilon = 0$ 14
- 3.6 My rendition of Figure 1.3 on page 4. This figure has all the same characteristics as Bender's original figure. All energies presented in this plot are real valued. The ϵ values are visible in the horizontal axis, while the vertical axis is the energy eigenvalues for each Hamiltonian in the parametric family $\hat{H} = \hat{p}^2 + \hat{x}^2(i\hat{x})^\epsilon$. The vertical dotted green line corresponds to the value $\epsilon = 0$, which itself corresponds to the 1D classical harmonic oscillator Hamiltonian $\hat{H} = \hat{p}^2 + \hat{x}^2$. Above the value $\epsilon = 0$ all values in the spectra are fully real, positive and discrete. Energy levels increase with increasing ϵ . In $-1 \leq \epsilon \leq 0$ region there is a finite number of real positive eigenvalues and an infinite number of complex-conjugate pairs of eigenvalues (the complex values are not depicted in this figure). The number of real eigenvalues decreases as ϵ decreases from 0 to -1, for ϵ values that are more negative than the value $\epsilon = -0.57793$ the only remaining real eigenvalue corresponds to the ground-state energy. At the value $\epsilon = -1$ the spectrum is null, as all eigenvalues diverge towards positive infinity. 15

- 4.1 The figure depicts the real-part of x in the horizontal axes, the imaginary-part of x in the vertical axes, a branch cut on the positive-imaginary axes, from zero to imaginary infinity, and four instances of *Stokes wedges* (one red and one yellow to differentiate between them) changing as functions of ϵ . For the cases when $\epsilon > 0$ the opening angles of the sectors decrease and the sectors rotate downward (both changes are respective to the $\epsilon = 0$ case). If $\epsilon = 0$, the angular opening is equal to $\pi/2$ and are centred about the positive-real and the negative-real axis. For the the cases of $\epsilon < 0$ the angular behaviour is opposite to the positive ϵ values. The wedges get wider and rotate upwards (both changes are respective to the $\epsilon = 0$ case) the changes, get more dramatic for decreasing ϵ values. In the case of $\epsilon = -1$ the wedges fuse into one along the logarithmic branch cut on the positive-imaginary line. We can describe the topology of this scenario as the logarithmic Riemann surface collapsing onto a single sheet. When this occurs, The spectrum becomes null, meaning that there are no eigenvalues at all[1][6]. 17
- 4.2 Integration contour used in my implementation of the WKB method for the region $\epsilon \geq 0$, the real-part of the integrand is the horizontal axis, and the imaginary-part of the integrand is on the vertical axis. The turning point x_- is marked in green and the turning point x_+ is marked in red. I also mark the direction of integration along the contour as an orange arrow along the blue contour. The contour is continuous and closed within the complex x -plane. 18

Abstract

Non-Hermitian quantum mechanics is a robust extension to quantum theory based on the redefinition of the Hermiticity condition expected from operators in quantum mechanics. If only Hermiticity is replaced by PT -symmetry but all other postulates of quantum theory are preserved, the number of possible systems available to study using quantum theory is expanded. In this theoretical project I investigate the properties of a parametric family of non-Hermitian but PT -symmetric Hamiltonians. My main results are the reproduction of a figure showing the eigenvalue spectra of this family of Hamiltonians. The figure demonstrates a clear image of PT -symmetry and how the boundedness, reality and complexity of eigenspectra is directly dependent on the broken or unbroken quality of the Hamiltonians' PT -symmetry. The figure exhibits several non-Hermitian spectral degeneracies known as exceptional points. In this work I also create a visualisation of the behaviour of two eigenstates for the family of parametric Hamiltonians. In this visualisation it is possible to see how the structure of the eigenstates changes in the regions of broken PT -symmetry specifically, as the states approach the parametric value corresponding to an exceptional point. By varying the parameter that characterizes the Hamiltonians, I demonstrate that the states behave as mirror images of each other in the parametric region past the exceptional point value, but the states are themselves symmetric about zero before crossing the exceptional point.

Chapter 1

Introduction

When my supervisors offered me the possibility of doing my research project on a different kind of quantum theory, I accepted the proposition promptly. From early on, my main motivation was to disenfranchise myself from any assumptions about what it meant to do quantum mechanics. I thought that this project could help me in the process of reformulating what I thought I already understood. This did happen, and the more I read about this topic the more I noticed that my picture of quantum theory was not wrong, but it was incomplete. From this realisation my curiosity only grew, as the new information I discovered resembled a set of shinier new tools for my toolbox. I hope that reading this work has the same effect for you.

1.1 Good ol' quantum mechanics

In the standard formalism of quantum mechanics operators must satisfy a set of properties which deem them suitable as real observable quantities in nature. An operator is defined as observable if its eigenvalues are real valued. This means that an observer may use the operator to measure certain qualities of a system and come to a real answer. In addition, it is necessary that the eigenvalues of the operator are bounded below. Hence, the observer will be able to measure a minimum value out of all the possible real answers. The original postulates of quantum mechanics encapsulate these two physical criteria in a mathematical property of operators known as Hermiticity (Hermitian operators are also known as self-adjoint operators in mathematics).

An operator \hat{O} is Hermitian if it satisfies for any $|f\rangle$ and $|g\rangle$

$$\langle f|\hat{O}|g\rangle = \langle g|\hat{O}|f\rangle^*, \quad (1.1)$$

Where the asterisk operation represents complex conjugation.

The equations governing the time evolution of a physical system can be derived from the Hamiltonian of said system[1]. Nominally, Hermitian Hamiltonians are used to describe systems that are not in contact with their environment. These idealised systems are conventionally called *closed* or *isolated*, these adjectives refer to the defined boundary conditions of the system and how these conditions affect the system dynamics. *Isolated* systems undergo unitary time evolution, i.e. As time passes, the eigenstates' norms are preserved and so the total probability of an eigenstate of the system is conserved.

The reality and boundedness of a Hermitian Hamiltonian's energy spectrum and the unitary time evolution of its eigenstates demonstrate the robustness of Hermiticity as a mathematical condition to impose as a postulate in quantum theory. But with this robustness arise limitations. Because it is not possible to use quantum theory on a system that is in contact with the outside environment.

1.2 Adopting a new assumption

The desire to study non-idealised systems using quantum mechanics requires that we reconsider the Hermiticity postulate and replace it with one that is less restrictive. In addition to expanding our analytical tool-box, non-Hermitian quantum mechanics prioritises physical principles rather than mathematical ones by establishing parity-time reflection symmetry (*PT*-symmetry) as a more generalisable alternative to Hermiticity.

1.3 PT -symmetric quantum mechanics

The P -operator represents parity (space-reflection), that is, any gain or loss components in a system get interchanged for the opposite component. The T -operator represents time-reversal, it has the effect of turning a system with gain into a system with loss (and vice versa)[1]. In Figure 1.1 on page 2, I present a toy example of a PT -symmetric system.

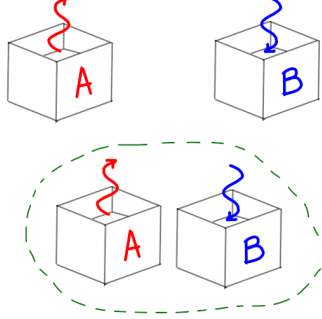


Figure 1.1: If there are two subsystems, call them A and B, and both subsystems are in contact with the outside environment, where the set-up is that the subsystem A gains energy while subsystem B loses the same amount of energy. Then we can consider the A and B subsystems as time-reversed versions of each other. Taken together as a larger combined system, then the AB system has no net probability flux. Notice that when we exchange A for B there is no change to the composite system, This means that the combined AB system is PT -symmetric.

The parity operator (P) is defined as a linear, reflection operator with the spatial basis matrix representation:

$$P = \begin{bmatrix} 0 & 1 \\ 1 & 0 \end{bmatrix}, \quad (1.2)$$

Notice that $P^2 = 1$. In addition, the P -operator is equal to its inverse $P = P^{-1}$.

The time-reversal symmetry operator (T) is defined as antilinear in order to preserve the Heisenberg commutation relation $[\hat{x}, \hat{p}] = i\hbar$ [1] and thus be consistent with the time dependent Schrödinger equation[2]. The antilinearity of T is defined as

$$T\psi T^{-1} = L\psi^*, \quad (1.3)$$

T acts as complex conjugation of a state ψ followed by a linear operator L (which may or not be Hermitian) acting on the state. There are two kinds of time-reversal: Even and odd, that is $T^2 = 1$ and $T^2 = -1$ respectively. These two kinds of time-reversal symmetry apply to different particles. In the case of Bosons (integer spin) only even T -symmetry applies. while odd T -symmetry applies exclusively to Fermions (half-integer spin)[2]. The scope of this work will focus exclusively in the case of even T -symmetry. With this simplification we can work with a basis such that

$$T\psi T^{-1} = \psi^*. \quad (1.4)$$

By focusing on even T -symmetry we can consider T as a reflection operator as we do with P . The T doesn't have a spatial basis matrix representation. Since parity and time-reversal operation are independent of each other, then the P and T operators commute[1].

In Figure 1.1 on page 2 we considered a very simple case of a composite PT -symmetric system, where the composition involved combining a subsystem A with its time-reversed version B. Let us imagine that A can be described with the simple 1×1 Hamiltonian $H_A = [a + ib]$ where $a, b \in \mathbb{R}$, since we established that B is simply the time-reversed version of A then B's Hamiltonian is $H_B = T(H_A)T^{-1} = [a - ib]$.

We can write the Hamiltonian of the composite AB system as the 2×2 Hamiltonian matrix

$$H_{AB} = \begin{bmatrix} a + ib & 0 \\ 0 & a - ib \end{bmatrix}. \quad (1.5)$$

H_{AB} is not Hermitian, but we can prove that it is PT -symmetric:

$$PT(H_{AB})T^{-1}P^{-1} = \begin{bmatrix} 0 & 1 \\ 1 & 0 \end{bmatrix} T \begin{bmatrix} a + ib & 0 \\ 0 & a - ib \end{bmatrix} T^{-1} \begin{bmatrix} 0 & 1 \\ 1 & 0 \end{bmatrix}, \quad (1.6)$$

$$\therefore PT(H_{AB})T^{-1}P^{-1} = \begin{bmatrix} 0 & 1 \\ 1 & 0 \end{bmatrix} \begin{bmatrix} a - ib & 0 \\ 0 & a + ib \end{bmatrix} \begin{bmatrix} 0 & 1 \\ 1 & 0 \end{bmatrix} \quad (1.7)$$

$$\therefore PT(H_{AB})T^{-1}P^{-1} = \begin{bmatrix} a+ib & 0 \\ 0 & a-ib \end{bmatrix} \quad (1.8)$$

$$\therefore PT(H_{AB})T^{-1}P^{-1} = H_{AB} \quad (1.9)$$

The system described by equation (1.5) is not in dynamic equilibrium since as time evolves, the norm of the states of subsystem A decay and those of B grow. If we implement a coupling parameter g between our subsystems, then the states of A and B will be coupled and so we can write the composite coupled-state Hamiltonian as

$$H_{\text{coupled}} = \begin{bmatrix} a+ib & g \\ g & a-ib \end{bmatrix} \quad (1.10)$$

Notice that PT -symmetry is preserved in equation (1.10). The coupling strength g determines the reality of the eigenvalue spectrum of H_{coupled} . To see this, we solve the eigenvalue problem

$$\det(H_{\text{coupled}} - IE) = a^2 + b^2 + E^2 - g^2 - 2aE \quad (1.11)$$

where I is the identity matrix and E are the eigenvalues we want to find. Notice that the second order polynomial in equation (1.3) is real. The roots of this polynomial are

$$E_{\pm} = a \pm \sqrt{g^2 - b^2}, \quad (1.12)$$

from this we can derive 3 scenarios, the first is the case when $g^2 < b^2$. In this case we have complex-valued eigenvalues, and so the weak coupling scenario yields a system that is not in dynamic equilibrium, because the coupled states continue to decay or grow. Alternatively, if $g^2 > b^2$ then this corresponds to strongly coupled states that do not decay nor grow, and so we have a real valued energy spectrum. These two coupling scenarios correspond to the cases of broken and unbroken PT -symmetry respectively. Finally the last case is when $g = \pm b$. This is the degenerate case. In non-Hermitian system degeneracy is expressed by real eigenvalues merging into complex conjugate pairs as $|g| \rightarrow b$. In my discussion I will explain on how the merging of eigenvalues has important experimental consequences.

1.4 Nerd-Sniped

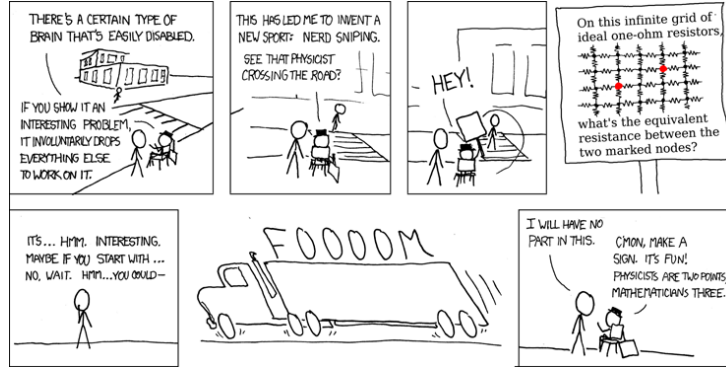


Figure 1.2: The relevant XKCD comic -Nerd Sniping- <https://xkcd.com/356/>. Illustrates what happened to me during my project.

I must be honest, I had a couple of ideas for my project but I only achieved one of them. Early on in the semester while I was reading “Making sense of non-Hermitian Hamiltonians” by Carl Bender I encountered a really interesting figure.

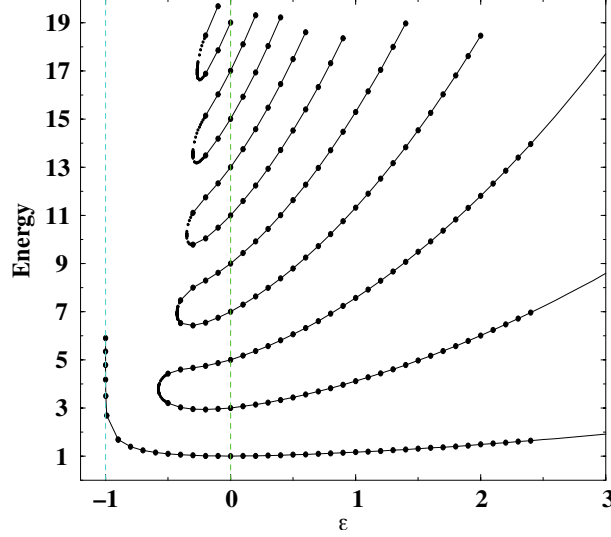


Figure 1.3: This is Figure 1. in reference [3]. It exemplifies the behaviour of the eigenvalue spectra of the general parametric family of non-Hermitian Hamiltonians $\hat{H} = \hat{p}^2 + \hat{x}^2(i\hat{x})^\epsilon$ as a function of the real parameter ϵ . All the eigenvalues visible in this figure are real valued. The PT -symmetry breaks at the $\epsilon = 0$, which corresponds to the Hamiltonian for the classic one dimensional harmonic oscillator. When $\epsilon \geq 0$ the spectra are real, positive and discrete. Energy levels increase with increasing ϵ . In the region corresponding to $-1 \leq \epsilon \leq 0$ there is a finite number of real positive eigenvalues and an infinite number of complex-conjugate pairs of eigenvalues (not depicted). The number of real eigenvalues decreases as ϵ decreases from 0 to -1 , for ϵ that are more negative than the value $\epsilon = -0.57793$ the only remaining real eigenvalue corresponds to the ground-state energy. At the value $\epsilon = -1$ the spectrum is null, as all the eigenvalues diverge to infinity.

My investigations of non-Hermitian Hamiltonians were pivoted by trying to understand what was going on in the figure above. My approach to understanding was based on trying to replicate the figure itself as it portrays a very clear visualisation of PT -symmetry breaking (occurring at $\epsilon = 0$) and its effect on the energy spectrum of non-Hermitian PT -symmetric Hamiltonians $\hat{H} = \hat{p}^2 + \hat{x}^2(i\hat{x})^\epsilon$. It can be seen in this figure that the reality and boundedness from below of the eigenvalues is maintained as the perturbation parameter ϵ is varied.

For my investigation of this figure, I had to solve the time independent eigenvalue problems associated with a $\hat{H} = \hat{p}^2 + \hat{x}^2(i\hat{x})^\epsilon$. For this I used two different mathematical techniques, since the reality of the spectrum for PT -symmetric Hamiltonian systems is characterized by the commutation relation of the Hamiltonian in question and the PT -operator. Because the PT -operator is non-linear, the eigenstates of the Hamiltonian may or may not be eigenstates of the PT -operator. We can establish the meaning of broken and unbroken PT -symmetry as a conditional statement: *If the Hamiltonian and the PT -operator share all eigenstates, then the symmetry is unbroken, but if not all the eigenstates are simultaneously shared between the Hamiltonian and the PT -operator then the symmetry is broken.*[1][3]. In other words, only if the PT -symmetric Hamiltonian shares eigenstates with the PT -operator, then the corresponding eigenvalues to those shared eigenstates are real-valued.

Replicating this figure took most of my time during the semester, and so I was unable to develop my other investigations further. Nevertheless, for the sake of completeness, I will describe in section 2 what my other project idea was.

Chapter 2

My aborted simulation

2.1 Methods

According to “Non-Hermitian quantum mechanics” by Nimrod Moiseyev. A book that I was given by my supervisors early on in the semester. The numerical propagation of wave packets is much more simple when taken within the framework of the non-Hermitian formalism of quantum mechanics rather than in the standard (Hermitian) formalism[4]. The main idea behind this method is to include a reflection-free complex absorbing potential (RF-CAP) in the Hamiltonian describing the wave packet’s time evolution. This added potential term allows the description of outward flowing states without any un-physical reflection effects from the boundary of the simulation region.

I was very eager to verify this technique on a simulation of a wave packet propagating in space using Python. First, I constructed wave function to be propagated. Since I required analytically verifiable derivatives, I figured that the easiest wave function choice was a Gaussian wave packet with initial condition

$$\psi(x, 0) = e^{-(x^2/2\sigma^2)} e^{ik_0 x}, \quad (2.1)$$

where $x \in \mathbb{R}$, $\sigma = 1$ and $k_0 = 10$. In order to implement the time evolution of my wave function, I used the 1D Schrödinger equation

$$\frac{d}{dt}\psi(x, t) = \frac{-i}{\hbar} \left[\frac{-\hbar^2}{2m} \frac{d^2}{dx^2} + V(x, t) \right] \psi(x, t), \quad (2.2)$$

To numerically calculate the second order spatial derivative I used the Fourier transform property $\mathcal{F}\{f'(x)\} = ik\mathcal{F}\{f(x)\}$, then my equation became

$$f(x, t, \psi) = \frac{-i}{\hbar} \left[\frac{-\hbar^2}{2m} \mathcal{F}^{-1}\{-k^2 \mathcal{F}\{\psi(x, t)\}\} + V(x, t)\psi(x, t) \right], \quad (2.3)$$

I was originally unsure of what the potential $V(x, t)$ should look like since the whole point of this exercise is the inclusion of a reflection-free complex absorbing potential (RF-CAP) in the Hamiltonian. The RF-CAP should attain non-zero values only in the boundary region in the coordinate space where the physical potential $V(x, t)$ vanishes[4]. Eventually, I opted for implementing a square well potential as $V(x, t)$ to give rise to the required non-physical interference that should be expected at the spatial boundaries of this problem. I defined the square well potential $V(x, t)$ as an array over an x-array ranging from 0 to 10. The square potential was defined as zero everywhere except at the boundaries. The boundaries’ height was determined by trial and error based on the kinetic energy of the wave packet. I settled with having the barrier to be a thousand times larger than the initial value for the wave vector squared, ie. $V(0, t) = V(10, t) = 1000k_0^2$.

To implement the time evolution required by the simulation I used the fourth-order Runge-Kutta method

on equation (2.3) $f(x, t, \psi)$. The algorithm is defined as

$$\begin{aligned}
k_1 &= f(x, t, \psi), \\
k_2 &= f(x, t + \frac{\Delta t}{2}, \psi + \frac{1}{2}k_1), \\
k_3 &= f(x, t + \frac{\Delta t}{2}, \psi + \frac{1}{2}k_2), \\
k_4 &= f(x, t + \Delta t, \psi + k_3), \\
\psi_{n+1} &= \psi_n + \frac{1}{6}(k_1 + 2k_2 + 2k_3 + k_4) + O(\Delta t^5).
\end{aligned} \tag{2.4}$$

where $\Delta t = 0.0001$ is the evolution time step, I chose this value to be small enough to be able to resolve motion of the Nyquist mode within the spatial step $\Delta x = \frac{x_{\max} - x_{\min}}{1024} = \frac{10}{1024}$. The numerical formula in equation (2.4) propagates a solution over a time interval, by solving a differential equation using four Euler-style steps (each involving one evaluation of the differential equation with slightly different parameters), and then combining the information obtained for each solution to match a Taylor series expansion up to fourth order. By combining the evaluations of the differential equation in this way we eliminate the error terms order by order, leaving the error remaining being very small[5].

2.2 Results

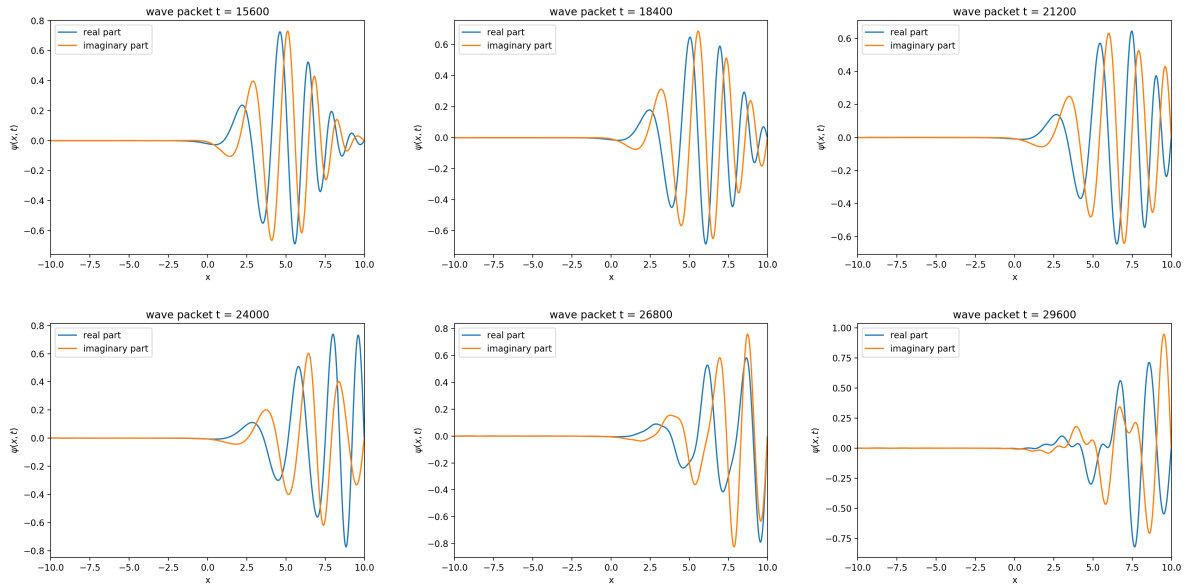


Figure 2.1: These are 6 frames of my simulation of a right propagating Gaussian wave packet in space as a function of time. The horizontal axes of every frame correspond to the spatial coordinate x (dimensionless) and the vertical axes of every frame correspond to the real and imaginary parts of the Gaussian wave packet. The earliest time frame is the top left panel, corresponding to wave packet at time $t = 15600$ as can be seen in that plot's title. The panels in this arrangement should be studied from left to right and top to bottom. An “undesirable” reflection of the real part of the wave packet at the boundary is visible specially in the last 3 frames from left to right, corresponding to times $t = 24000$, $t = 26800$ and $t = 29600$ as can be seen in the plots' titles from left to right respectively.

Understanding the implementation of the potential characteristic to this non-Hermitian technique simulation required a lot of reading and I ambitiously decided to leave this project unfinished in the meantime and continue with it after I successfully replicated Figure 1. in Bender. A project which I naively expected to finish quickly.

Chapter 3

Reproducing Bender's figure

The defining principle behind Figure 1.3 on page 4 is that we can think of the family of non-Hermitian PT -symmetric Hamiltonians defined below as complex deformations of the 1D harmonic oscillator (which is Hermitian and PT -symmetric).

$$\hat{H} = \hat{p}^2 + \hat{x}^2(i\hat{x})^\epsilon, \quad (3.1)$$

where ϵ is a real parameter. The introduction of the real parameter ϵ acts in such a way that as ϵ increases from 0, the Hamiltonian is no longer Hermitian but its PT -symmetry is preserved. This occurs because the quantity $(i\hat{x})$ is PT -invariant[1][3].

To formulate the eigenvalue problems for both methods used to find all the eigenvalues of equation (3.1), I split the problem into the expected parametric regions (as per Bender's descriptions) corresponding to *unbroken* PT -symmetry ($\epsilon \geq 0$) and *broken* PT -symmetry ($\epsilon < 0$).

When $\epsilon \geq 0$ the spectra are real, positive and discrete. Energy levels increase with increasing ϵ . To solve the Schrödinger eigenvalue problem I write the Schrödinger equation in coordinate space.

The relevant operators in this space are

$$\hat{x} \rightarrow x, \quad \hat{p} \rightarrow -i\frac{d}{dx}, \quad (3.2)$$

where we want to treat the variable x as complex, which does not modify the commutation relation $[\hat{x}, \hat{p}] = i\hbar$. Without loss of generality we can use natural length scales ($\hbar = 1, m = \frac{1}{2}$) so the eigenvalue problem takes the form

$$-\psi'' + x^2(ix)^\epsilon\psi = E\psi. \quad (3.3)$$

Equation (3.3) cannot be solved exactly using analytic methods for $\epsilon \neq 0$, therefore my approach is numerical. From reference [3] I learned that the WKB phase integral approximation can be used to find very a accurate approximation to the real eigenvalues visible in the *unbroken* PT -symmetry region ($\epsilon \geq 0$) visible in Figure 1.3 on page 4.

3.1 Methods

3.1.1 WKB approximation

To solve equation (3.3) I had to find out which were the boundary conditions for the problem. I learned from several sources that the boundary conditions depend on the deformation parameter ϵ [1][3][6]. Since the eigenvalue problem can be conceptualised as a harmonic oscillator that has been deformed into the complex x -plane we need to re-frame the spatial variable x as $x = re^{i\theta}$, finding the solutions requires that I integrate equation (3.3) along a contour in the complex x -plane and that the solution be equal to zero at both ends of this contour[1]. According to Bender, the integration contour should be located within two angular sectors in the complex x -plane as $|x| \rightarrow \infty$. These sectors are called *Stokes wedges*[1][3], in general these wedges are centred about the origin in the complex x -plane and we can define their orientation the complex x -plane in terms of

$$-\frac{1}{4}\pi < \theta < \frac{1}{4}\pi \quad \text{and} \quad \frac{3}{4}\pi < \theta < \frac{5}{4}\pi \quad (3.4)$$

the eigenfunctions of the problem vanish exponentially at both ends of the integration contour. Determining the locations of the *Stokes wedges* is in general not necessary to solve the differential equation

exactly[1]. For the purpose of my eigenvalue problem, it is only required to understand the asymptotic behaviour of the solutions for large $|x|$ values.

I assumed that for an ODE of the form of equation (3.3), ie. $\psi''V(x)^\epsilon\psi = E\psi$, the behaviour of $(E - V(x)) \rightarrow \infty$ as $|x| \rightarrow \infty$ in the complex x -plane. The next assumption I made was that the solution should be of the form

$$\psi \approx \exp[\pm \int^x dx \sqrt{E - V(x)}], \quad (3.5)$$

this is called the *geometrical-optics approximation*[1].

The location of *Stokes wedges* in the complex plane, and hence the defined boundary conditions for my problem are determined by imposing that $\psi(x) \rightarrow 0$ as $|x| \rightarrow \infty$ similarly to the case where $\epsilon = 0$ ie. The classical harmonic oscillator case, where the solutions are known to be square integrable for real x -values. Since I am assuming that my solutions will be wave functions moving in space, I am interested in learning how much phase is gained by traversing the integration contour in the complex x -plane. The end points of the integration contour are the turning points (the roots of the equation $E = x^2(ix)^\epsilon$) that *analytically continue off* of the real axis as ϵ increases from 0[1][3]. Independently of the number of possible roots of $E = x^2(ix)^\epsilon$, for the purpose of my technique I only need the following turning points to be the limits of integration

$$x_- = E^{\frac{1}{\epsilon+2}} e^{i\pi(\frac{3}{2} - \frac{1}{\epsilon+2})} \quad \text{and} \quad x_+ = E^{\frac{1}{\epsilon+2}} e^{-i\pi(\frac{1}{2} - \frac{1}{\epsilon+2})}. \quad (3.6)$$

The explicit formula I used in my numerical calculation of the eigenvalues is the the leading order WKB phase integral quantization condition

$$\left(n + \frac{1}{2}\right) \pi = \int_{x_-}^{x_+} dx \sqrt{E - x^2(ix)^\epsilon}, \quad (3.7)$$

as per Bender's instructions in "Making sense of non-Hermitian Hamiltonians". the left hand side of equation (3.7) is the quantization condition on the accumulated phase for the WKB integral that defines the energy.

Since it does not make sense to compute a complex integral in Python, I proceeded with my numerics by implementing a change of variables that shifted my integration limits and domain from the complex plane to the real line. I did this taking advantage of the symmetry of the set-up. Because both turning points x_\pm have equal imaginary parts, I subtracted the imaginary part multiplied by i from both of the integration limits and also added it to the complex x value present in the integrand as an offset

$$\begin{aligned} x_- &\rightarrow x'_- = x_- - i\text{Im}(x_-), \\ x_+ &\rightarrow x'_+ = x_+ - i\text{Im}(x_-), \\ x &\rightarrow x = x' - i\text{Im}(x_-), \\ dx &\rightarrow dx'. \end{aligned} \quad (3.8)$$

After my change of variables, I was able to calculate the WKB integral by writing my own integration function and using the *quad()* module for integration in Python. I wrote a modified function that calculated integral for the real part and the integral for imaginary part of the integrand separately and set the function to return the total integral as a linear combination of the real plus i times the imaginary part. I named my function: *complex_quad()*.

I was able to verify the quantisation condition in equation (3.7) by taking the difference of the expression dependent of n in the left hand side of equation (3.7) and the resulting complex integral I calculated by using my *complex_quad()* function which corresponds to the right hand side of equation (3.7). I used this difference equation to optimize the resulting energy eigenvalue from my *complex_quad()* function. For the optimization I used my own modified version of the root finding algorithm module *scipy.optimize.fsolve()*. My modifications simply allowed me to use the algorithm for both the real and imaginary part of my results, and to combine them similarly to what I did when calculating the real and imaginary parts of the complex integral as two separate integrals.

3.1.2 Matrix equations

The process I followed to solve equation (3.3) for the broken PT -symmetry region (the region corresponding to values of $\epsilon < 0$) was a lot more free form. Bender's paper "Making sense of non-Hermitian Hamiltonians" did not go into details about the behaviour of the spectrum this region nor gave any advice

on how to solve the eigenvalue problem for the parametric Hamiltonians with $\epsilon < 0$ values. I chatted to my supervisors a lot when I was working on this and we settled on me attempting to re-write equation (3.3) as a matrix equation using the family of harmonic oscillators eigenstates written in the x-spatial coordinate the basis. These functions are also known as Hermite functions and are generally written as

$$\psi_n(x) = \frac{1}{\sqrt{2^n n!}} \left(\frac{m\omega}{\pi \hbar} \right)^{1/4} e^{-\frac{m\omega x^2}{2\hbar}} H_n \left(\sqrt{\frac{m\omega}{\hbar}} x \right), \quad n = 0, 1, 2, \dots \quad (3.9)$$

where the functions $H_n(z)$ are the physicists' Hermite polynomials

$$H_n(z) = (-1)^n e^{z^2} \frac{d^n}{dz^n} \left(e^{-z^2} \right). \quad (3.10)$$

In equation (3.3) I have used natural length scales, ie. $\hbar = 1, m = \frac{1}{2}$. To simplify my states further, I set the frequency in my harmonic oscillator basis states to $\omega = 2$ to obtain

$$\psi_n(x) = \frac{1}{\sqrt{2^n n!}} \left(\frac{1}{\pi} \right)^{1/4} e^{-\frac{x^2}{2}} H_n(x). \quad (3.11)$$

To numerically solve my matrix equation I first needed to calculate N (I chose $N = 100$) harmonic oscillator basis states as they are written in equation (3.11), and then I used them to form the matrix elements

$$\langle m | \hat{H} | n \rangle = \int_{-b}^b \psi_m(x)^* \left(-\frac{d^2}{dx^2} + x^2(ix)^\epsilon \right) \psi_n(x) dx \quad (3.12)$$

where m and n are the indices for the harmonic oscillator states. Both m, n range from 0 to 100, and $\pm b$ are the integration limits which I will define in the next section. Using these elements I constructed one hundred Hamiltonian matrices. Each Hamiltonian matrix corresponds to a different ϵ value in a range of one hundred values between 0 to -1. After the matrices were constructed I simply used the *scipy.linalg.eig()* module in Python to solve each eigenvalue problem for my set of 100×100 Hamiltonian matrices. With this module I found the eigenvalues and the right eigenvectors for each matrix.

Matrix elements

An important part of my integral calculations was the need to choose the integration region for each matrix element. I needed the largest possible region without compromising the time spent for each element integration and so the integration bounds must depend on the state with the highest energy value used for each of the one hundred elements calculated. In addition, I needed to make sure the states went to zero for large x -values in order to take advantage of the basis states. Therefore I set the limits of integration to be much larger than the turning points of the harmonic oscillator so I was able to guarantee that the states have exponentially decayed to zero at the bounds of my integration. I settled the boundaries by trial and error and determined that the values $b = \pm \sqrt{4\min(m, n) + 2} + 2$ were more than adequate.

To iteratively calculate the matrix elements as they are written in equation (3.12) I once again, used the *complex.quad()* function I wrote myself since the integrand of each matrix element integral was complex-valued. My modified function calculates the integral for the real part and the integral for imaginary part of the integrand separately and it returns the total integral as a linear combination of the real plus i times the imaginary part.

Finally, my code repeated this procedure and calculated one hundred 100×100 matrices. One matrix for each ϵ in my discretised region for ϵ values between 0 and -1.

Constructing the integrand for each matrix element as per equation (3.12), was computationally expensive, because it required the calculation of the harmonic oscillator basis states ψ_m and ψ_n , and that of the Hamiltonian. To numerically calculate the second order derivative in the Hamiltonian I used a finite centred differences approximation

$$\frac{d^2 \psi_n(x)}{dx^2} = \frac{\psi_n(x+h) - 2\psi_n(x) + \psi_n(x-h)}{h^2} \quad (3.13)$$

I calculated $\psi_m(x)$ once for every integrand, but I calculated 3 different $\psi_n(x)$ for my centred finite differences, meaning that my algorithm was complexity $O(N^3)$.

I will explain now why this approach crashed my calculation.

Hermite functions

The main computational issue was due to the size of the Harmonic oscillator states $\psi_n(x)$. The factors that comprise the states are: $\frac{1}{\sqrt{2^n n!}}$ which underflows as n grows large, and the Hermite polynomial $H_n(x)$ which overflows as n grows large. This behaviour makes numerically generating high n harmonic oscillator states impossible (high n can be as low as $n = 130$). I solved this problem using a modified version of a numerical method available in www.numbercrunch.de written by H. Bauke. The aim of the method is to calculate the functions in equation (3.11) using the recurrence relation

$$H_n(x) = 2xH_{n-1}(x) - 2(n-1)H_{n-2}(x) \quad (3.14)$$

where $H_0(x) = 1$ and $H_1(x) = 2x$. The recursion relation partly eliminates the blow up of equation (3.11) by taking care of the issue due to large values of n . Therefore the method defines the recurrence relation corresponding to equation (3.11) as

$$\psi_n(x) = \sqrt{\frac{2}{n}}x\psi_{n-1}(x) - \sqrt{\frac{n-1}{n}}(n-1)\psi_{n-2}(x) \quad (3.15)$$

Lastly, to fully solve all problems of underflow and overflow it is necessary to consider what happens when we are dealing with Hermite functions at large x values. For $x > 38$ the factor $e^{-x^2/2}$ is smaller than any number that can be represented as a double precision floating point number. A very robust remedy to numerical underflow was sketched in BIT Numerical Mathematics, Vol. 49, pp 281-295. The basic idea is to keep the magnitude of the modified Hermite polynomials on the order of one during their calculation via the recurrence relation (3.15) by introducing a suitable normalizing factor. During the calculation one has to keep track of the sum of the logarithms of these normalizing factors. Then the factor $e^{-x^2/2}$ has to be modified by this sum when the value of the Hermite function is calculated. This algorithm allows to calculate the values of high-order Hermite functions even for quite large arguments[7].

Once I implemented the changes to my code suggested by Bauke's work, my matrix elements were actually computed but the speed of each integral I calculated was incredibly slow. My numerics required some Cython to allow the code to compile the function using C in order to bypass the limitations that come from using exclusively Python. My partner Chris helped me with this step and he translated my code into Cython for me. The algorithm is still the same complexity as before ($O(N^3)$) but the calculations were compiled approximately $380\times$ faster than when I used Python code. Still, to discretising my range of ϵ I decided to use 100 values, so I had to calculate one hundred Hamiltonian matrices. This required that the code ran overnight.

Visualising eigenstates in the broken PT -symmetry region

Jesper suggested that I made an animation to illustrate how the wave functions of the Hamiltonian in equation (3.1) change as ϵ change along the solutions in the energy ϵ diagram. The main motivations for crating this animation were first, to verify if the eigenvectors were orthogonal, because the complex eigenstates of a non-Hermitian system are, in general, not orthogonal. And second, because we wanted to observe the coalescent behaviour of the eigenstates present in the broken symmetry region of the spectrum. We were curious to see how an eigenfunction continuously becomes another, and we were also intrigued by the point at which this transformation would be visible.

First I decided to exclusively use the first and second excited states for the Hamiltonian in equation (3.1), I chose these because I can see that these states certainly coalesce in both Figure 1.3 on page 4 and my own rendition, visible in section 3.2.4. I needed to sort the eigenstates list using the indices of the second and third elements of the sorted eigenvalues list. To do this, I used Boolean arrays to conditionally select the eigenvalues that satisfied some filtering and sorting conditions. I filtered all the eigenvalues by requiring that the real-parts were between 0 and 20. and imposed this indexing condition on the list of eigenstates, which lead to the eigenstate list to be sorted corresponding to the desired eigenvalues in the range $0 < E < 20$. After this, I sorted the eigenstates by using `np.argsort()` to return the indices that would sort the array based on the eigenvalue array. This module performs an indirect sort along the given axis using the algorithm specified by the kind keyword. My sorting key used the rounded real-part of the eigenvalues up to 3 significant figures plus the scaled by one in a millionth rounded imaginary-part of the eigenvalues up to 3 significant figures. This condition allowed the sorting to be principally influenced by

the real-part of the eigenvalue and only be influenced by the imaginary part if the real parts were exactly equal. The `np.argsort()` module returns an array of indices of the same shape as a that index data along the given axis in sorted order[8].

After the filtering and sorting of eigenstates, I needed to normalise the states by

$$\psi_{jx} = \frac{\psi_{jx}}{\sqrt{\sum_i |\psi_{x_i}|^2 \Delta x}}, \quad (3.16)$$

where ψ_{x_i} are the individual points forming the wave function.

Since the eigenstates might be returned with an arbitrary phase. In order to avoid ugly discontinuities in my plot frames I want to eliminate these arbitrary phases by multiplying the state by the exact opposite phase factor.

$$\psi_{jx} = \psi_{jx} e^{-i \text{Arg}(\psi_{jx})}, \quad (3.17)$$

Finally, I obtained one hundred plots that were to be used as animation frames for my oral presentation. I also made some plots to observe how the probability amplitudes of the eigenstates behaved as ϵ ranged between -1 and 0.

3.2 Results

3.2.1 The region of unbroken PT -symmetry

Using the WKB integral quantisation condition I calculated how much phase is gained by traversing a contour in the complex plane from one of the roots of the equation $E = x^2(ix)^\epsilon$ to another. Here I compare my numerical results for the energies pertaining to the unbroken PT -symmetry region ($\epsilon \geq 0$) in Figure 1.3 on page 4 with the energies reported in Bender's paper "Making sense of non-Hermitian Hamiltonians" by plotting my obtained energy values together with Bender's calculated numerical energies, Bender's values are reported to have been obtained by the WKB integral and by Runge-Kutta.

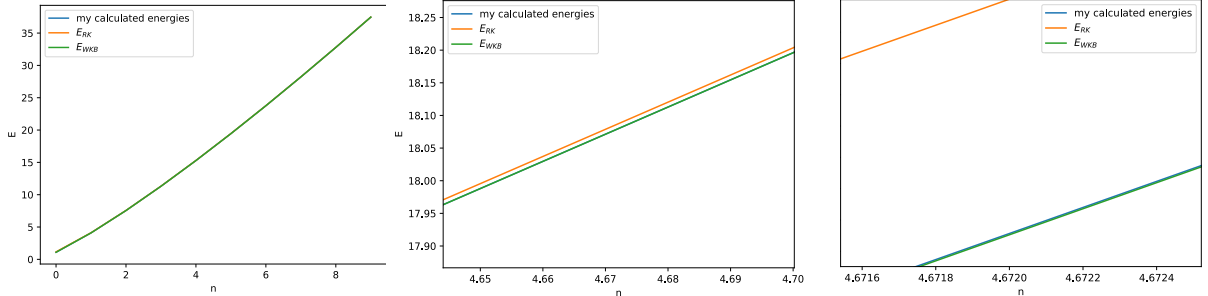


Figure 3.1: From left to right the image is zoomed. Here I demonstrate that my WKB energy results (visible as the blue plot) for the case on the non-Hermitian, PT -symmetric Hamiltonian $\hat{H} = \hat{p}^2 + \hat{x}^2(ix)$ (ie. the case: $\epsilon = 1$) are in agreement with the energy values reported in Bender's work. Bender's results were obtained by the Runge-Kutta method (orange plot) and by the WKB approximation (green plot). All the energies (energy is the vertical axis) presented in this plot were obtained using $n \in [0, 9]$. n is visible as the horizontal axis for this plot.

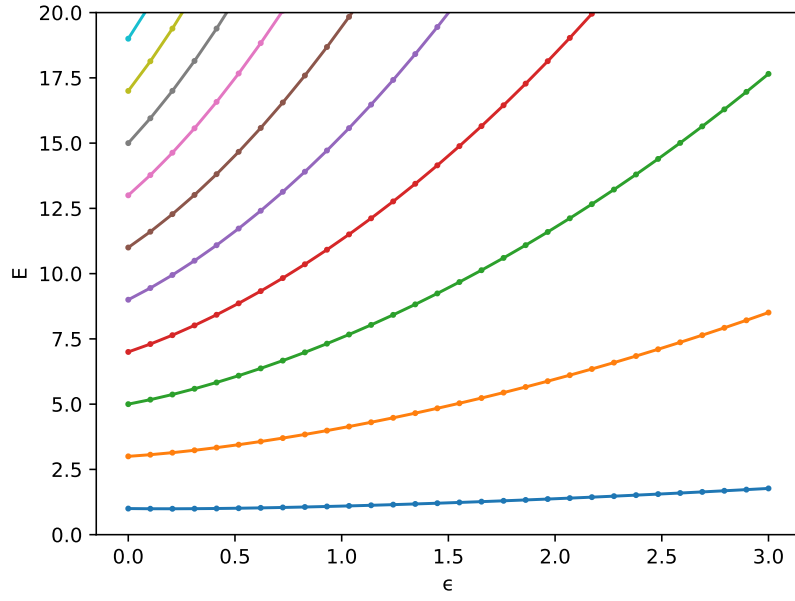


Figure 3.2: My implementation of the WKB method on the family of non-Hermitian, PT -symmetric Hamiltonians $\hat{H} = \hat{p}^2 + \hat{x}^2(i\hat{x})^\epsilon$ for $\epsilon \geq 0$. My energy values (energy is the vertical axis) were in agreement with those visible in Figure 1.3 on page 4. All the energies presented in this plot are real valued, and they are bounded below by the eigenvalues corresponding to the ground-state visible here as a blue plot. The changing colours of every plot represent increasing values of n corresponding to the left hand side expression in the WKB quantisation condition: $(n + \frac{1}{2})\pi$. The horizontal axis is the range of values $0 \leq \epsilon \leq 3$.

3.2.2 The region of broken PT -symmetry

I solved the eigenvalue problem presented in equation (3.3) for one hundred different parametric Hamiltonians as per equation (3.1). I obtained my numerical results for the eigenvalue spectra of each Hamiltonian for one of the ϵ values in the discretised range of a hundred values ranging from 0 to -1. My obtained energy values matched the plotted energies reported in Bender's paper "Making sense of non-Hermitian Hamiltonians", and Bender et al. "Behaviour of eigenvalues in a region of broken pt symmetry".

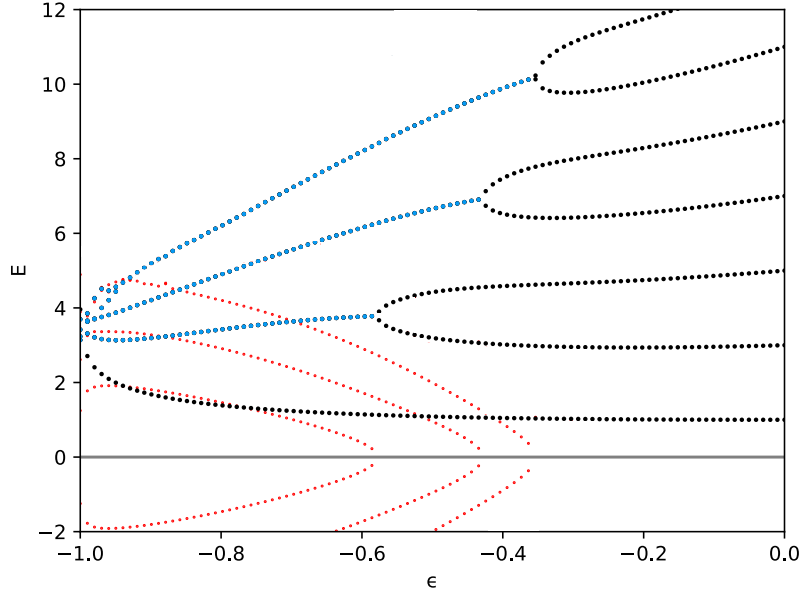


Figure 3.3: This plot is an extension of Figure 1.3 on page 4. Here I display the discretised space of ϵ as 100 values in the horizontal axis, and the eigenvalues of the parametric family of PT -symmetric, non-hermitian Hamiltonians $\tilde{H} = \hat{p}^2 + \hat{x}^2(i\hat{x})^\epsilon$ for the region corresponding to $\epsilon \leq 0$ in the vertical axis. This figure depicts fully real eigenvalues (black dots) and the points at which the eigenvalues become degenerate and then form complex-conjugate pairs. The real parts of these pairs of eigenvalues (blue dots) initially decrease as ϵ decreases but blow up suddenly as ϵ approaches -1. The imaginary parts of the eigenvalue pairs (red dots) remain finite and appear to decay to zero at $\epsilon = -1$.

3.2.3 The behaviour of eigenstates

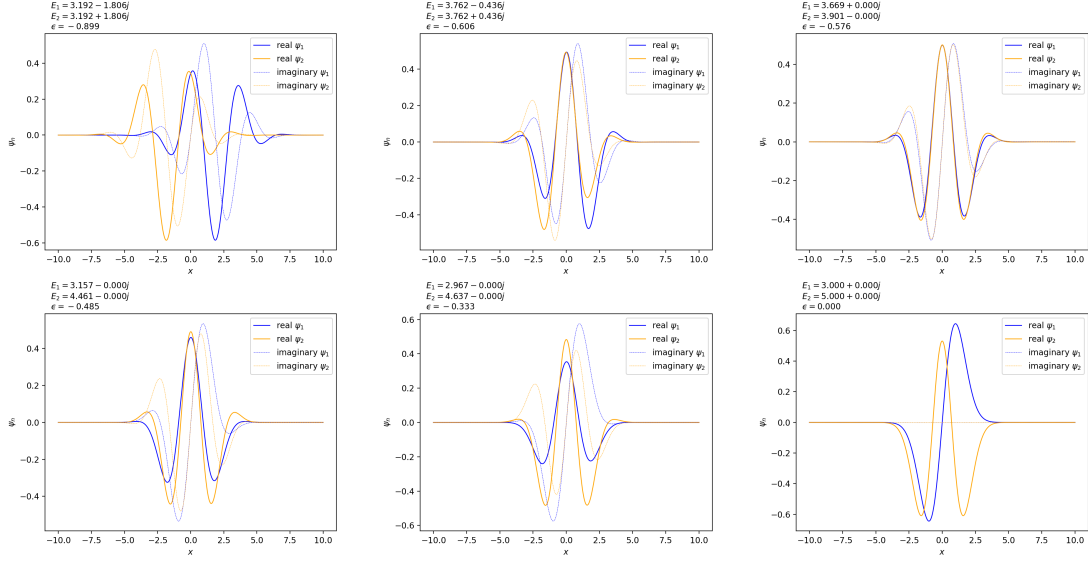


Figure 3.4: These are 6 frames in the visualisation of the behaviour of the first and second excited states for the Hamiltonian in equation (3.1) in the region of broken PT -symmetry. The horizontal axes of each plot represent the x coordinate, and the vertical axes represent the wave functions. In addition to the legend I have added on the top left corner of each of the plots the corresponding eigenvalues to each of the wave functions, and the corresponding ϵ value to make note of this parametric dimension. On the top left panel, the ϵ value is most negative. The plots in this arrangement should be studied from left to right and top to bottom. Here I demonstrate how the structure of the eigenstates changes as we approach the ϵ value corresponding to the **exceptional point** (approximately $\epsilon = -0.576$). As ϵ varies, we can see the wave functions behave as mirror images of each other when the ϵ value is more negative than the exceptional point. Then at the approximate value of the exceptional point (visible in the top right plot), the wave functions overlap. As the ϵ values become less negative than the exceptional point, the states themselves become symmetric about zero. At the bottom right plot, we see that the states are the first and second excited states of the harmonic oscillator, i.e. $\epsilon = 0$.

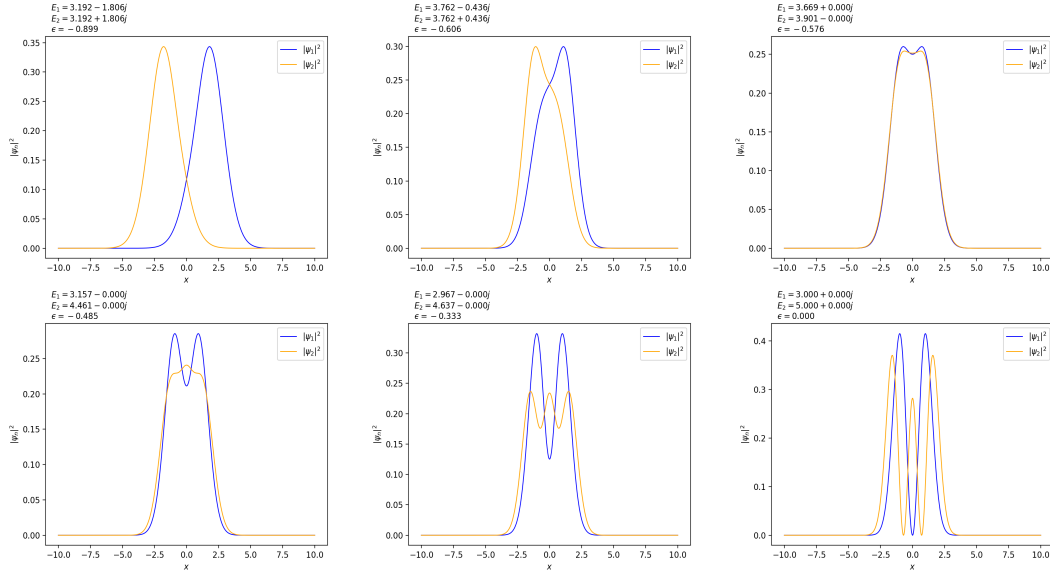


Figure 3.5: These are 6 frames in the visualisation of the behaviour of the probability density of the first and second excited states for the Hamiltonian in equation (3.1) in the region of broken PT -symmetry. Similarly to the previous figure, the horizontal axes of each plot represent the x coordinate, and the vertical axes represent the probability density of the states. In addition to the legend I have added on the top left corner of each of the plots the corresponding eigenvalues to each state, and the corresponding ϵ value to make note of this parametric dimension. On the top left panel, the ϵ value is most negative. The plots in this arrangement should be studied from left to right and top to bottom. Here I demonstrate how the eigenstates densities change as we approach the ϵ value corresponding to the **exceptional point** (approximately $\epsilon = -0.576$). As ϵ varies, we can see the densities behave as mirror images of each other when the ϵ value is more negative than the exceptional point. Then at the approximate value of the exceptional point (visible in the top right plot), the densities overlap. As the ϵ values become less negative than the exceptional point, the densities themselves become symmetric about zero. At the bottom right plot, we see that the states densities correspond to those of the first and second excited states of the harmonic oscillator, i.e. $\epsilon = 0$.

3.2.4 The full version of the figure

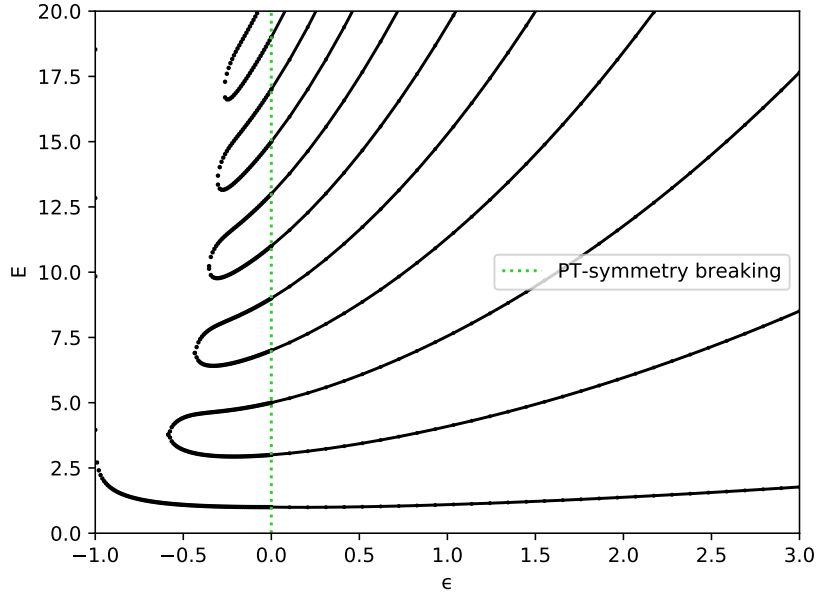


Figure 3.6: My rendition of Figure 1.3 on page 4. This figure has all the same characteristics as Bender's original figure. All energies presented in this plot are real valued. The ϵ values are visible in the horizontal axis, while the vertical axis is the energy eigenvalues for each Hamiltonian in the parametric family $\tilde{H} = \hat{p}^2 + \hat{x}^2(i\hat{x})^\epsilon$. The vertical dotted green line corresponds to the value $\epsilon = 0$, which itself corresponds to the 1D classical harmonic oscillator Hamiltonian $\tilde{H} = \hat{p}^2 + \hat{x}^2$. Above the value $\epsilon = 0$ all values in the spectra are fully real, positive and discrete. Energy levels increase with increasing ϵ . In $-1 \leq \epsilon \leq 0$ region there is a finite number of real positive eigenvalues and an infinite number of complex-conjugate pairs of eigenvalues (the complex values are not depicted in this figure). The number of real eigenvalues decreases as ϵ decreases from 0 to -1, for ϵ values that are more negative than the value $\epsilon = -0.57793$ the only remaining real eigenvalue corresponds to the ground-state energy. At the value $\epsilon = -1$ the spectrum is null, as all eigenvalues diverge towards positive infinity.

Chapter 4

Discussion

Since my main project objective became the calculation of the eigenvalues of a family of non-Hermitian, PT -deformed Hamiltonians, and to replicate the energy spectra figure published by Bender in “Making sense of non-Hermitian Hamiltonians”. I want to give a bit of an insight on the reasons why I opted for using certain numerical techniques over others.

4.1 Complex WKB

For the unbroken PT -symmetry region of the spectrum, I decided to follow Bender’s methodology in “Making sense of non-Hermitian Hamiltonians”. In the paper he describes the WKB approximation technique as yielding a good approximation to the exact energy values of the eigenvalue problem. However, I found the efficacy of its implementation in the complex plane to be quite unintuitive.

The complex WKB method involves treating x as a complex variable (ie. $x = re^{i\theta}$), and calculating how the asymptotic form of the solutions change as they are traced around the complex plane[9].

Since the integral in the exponent in equation (3.5) is in general, complex valued, the solutions will contain either growing or decaying exponential terms. The nomenclature of the solutions depends on these growing or decaying exponential terms (since they describe a particular asymptotic behaviour). The solutions are called either **dominant** or **sub-dominant** respective to these growing or decaying exponential terms.

If the integral in the exponent in equation (3.5) is purely real, then both WKB solutions will be purely oscillatory, with neither dominating the other[9].

The bounds (x_{\pm}) of the integral in equation (3.7) are turning points of the equation $P(x) = E - V(x)$. Lines can be drawn in the complex plane, emanating from the turning points, marking the curves where $\text{Im}(\int_{x_-}^{x_+} P(x)^{\frac{1}{2}} dx) = 0$. These lines are known as *Stokes lines* and they mark the borders between sectors in the complex plane where solutions undergo **dominant** or **sub-dominant** behaviour, these sectors are known as *Stokes wedges*. Knowing the position of *Stokes lines* is crucial in applying the complex WKB method[9].

4.2 Stokes wedges and boundary conditions

One aspect of the complex WKB method that I found quite unintuitive was the determination of the boundary conditions for the differential equation (3.3).

The WKB method works for the $\hat{H} = \hat{p}^2 + \hat{x}^2(i\hat{x})^{\epsilon}$ eigenvalue problems for values of $\epsilon \geq 0$ because the sub-dominant eigenfunctions vanish exponentially in two *Stokes wedges* in the complex x -plane. The eigenfunctions will vanish most rapidly at the centres of the wedges; at the edges of the wedges the eigenfunctions just oscillate and no longer vanish exponentially[1].

The *Stokes wedges* I studied are always centred about the origin of the complex x -plane. As I described in section 3.1.1, their angular orientation in the complex x -plane can be described by the argument of the complex variable $x = re^{i\theta}$.

The limits of integration used in the WKB technique are analogous to classical turning points. Ie. the total energy of the system obeys the equation $E = x^2(ix)^{\epsilon}$ and this equation has many complex solutions.

However, since we are interested in E being real, we are concerned with what happens to two turning points that lie on the real axis at $\pm\sqrt{E}$ when $\epsilon = 0$ as ϵ increases[1]. The form of the turning points I wrote in equation (3.6) is

$$x_- = E^{\frac{1}{\epsilon+2}} e^{i\theta_-} \quad \text{and} \quad x_+ = E^{\frac{1}{\epsilon+2}} e^{i\theta_+}, \quad (4.1)$$

where the angles are

$$\theta_- = \frac{4 + 3\epsilon}{4 + 2\epsilon} \pi \quad \text{and} \quad \theta_+ = -\frac{\epsilon}{4 + 2\epsilon} \pi. \quad (4.2)$$

This left-right reflection symmetry is the coordinate space realisation of PT -symmetry[1]. When ϵ increases from 0, the turning points move into the complex plane. Notice that the turning points are symmetric respect to reflections along the imaginary axis. This is a direct consequence of PT -symmetry[1]. As ϵ increases from 0, a logarithmic branch-point singularity appears at the origin, and as ϵ continues increasing in the positive direction, it is necessary to introduce a branch-cut running from the origin along the positive imaginary axis. In this cut plane the solutions to equation (3.3) are analytic and singled-valued[1].

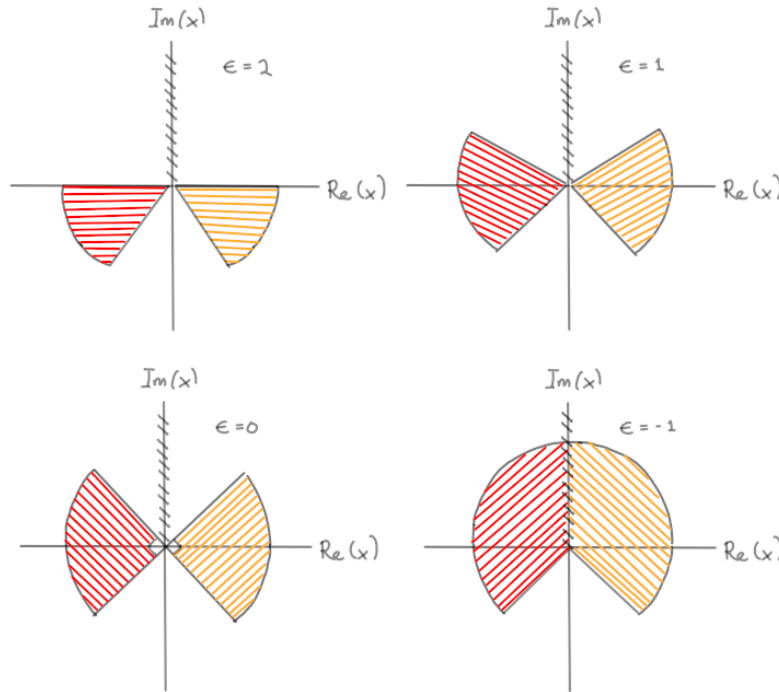


Figure 4.1: The figure depicts the real-part of x in the horizontal axes, the imaginary-part of x in the vertical axes, a branch cut on the positive-imaginary axes, from zero to imaginary infinity, and four instances of Stokes wedges (one red and one yellow to differentiate between them) changing as functions of ϵ . For the cases when $\epsilon > 0$ the opening angles of the sectors decrease and the sectors rotate downward (both changes are respective to the $\epsilon = 0$ case). If $\epsilon = 0$, the angular opening is equal to $\pi/2$ and are centred about the positive-real and the negative-real axis. For the the cases of $\epsilon < 0$ the angular behaviour is opposite to the positive ϵ values. The wedges get wider and rotate upwards (both changes are respective to the $\epsilon = 0$ case) the changes, get more dramatic for decreasing ϵ values. In the case of $\epsilon = -1$ the wedges fuse into one along the logarithmic branch cut on the positive-imaginary line. We can describe the topology of this scenario as the logarithmic Riemann surface collapsing onto a single sheet. When this occurs, The spectrum becomes null, meaning that there are no eigenvalues at all[1][6].

4.3 PT -symmetry breaking

Because of several coding errors I made, and in the process of fixing them I was able to explore the WKB integration method more deeply. I investigated the integration contour for the WKB integral by plotting it several times until I identified my integration issues. By following this process I verified that the turning points indeed form a closed loop of integration which follows the analogy of the classical interpretation of the turning points as the finishing and starting points of a moving classical particle.

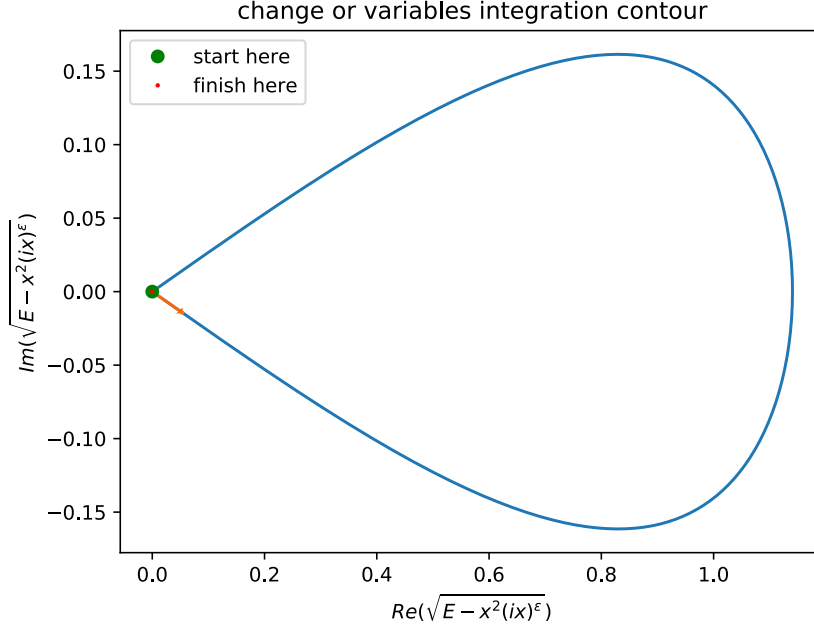


Figure 4.2: Integration contour used in my implementation of the WKB method for the region $\epsilon \geq 0$, the real-part of the integrand is the horizontal axis, and the imaginary-part of the integrand is on the vertical axis. The turning point x_- is marked in green and the turning point x_+ is marked in red. I also mark the direction of integration along the contour as an orange arrow along the blue contour. The contour is continuous and closed within the complex x -plane.

I explained in section 3.1.1 that to use the WKB approximation, it is necessary to impose $\psi \rightarrow 0$ as $|x| \rightarrow \infty$ along the integration contour located within two angular sectors in the complex x -plane.

We encounter a problem as ϵ becomes negative, because there is no continuous path joining the limits of integration used in the WKB approximation, therefore we cannot use this technique in the region with broken PT -symmetry.

To solve the eigenvalue problem for this region, ie. the region corresponding to $\epsilon < 0$, I originally had an idea for developing the numerics of this region based on the shooting method[5], Unfortunately this idea was difficult to implement given that I was dealing with a complex equation, and so it was not exactly clear to me how I should use this method. Eventually, opted to discretise the range $-1 \leq \epsilon < 0$ and proceeded to solve the eigenvalue problems for each resulting parametric Hamiltonian as a matrix equation.

I faced a few complications using the matrix method. Initially my intuition was that the matrices should be dimensionally large so I would get more resolution in the Harmonic oscillator space, because the more eigenstates I use the more degrees of freedom I should have which would mean that my eigenvalue calculations of the non-Hermitian Hamiltonians would be more accurate. The issue was that if I increased the number of states used to make my matrix the number of eigenvalues will increase linearly with N and I only wanted to have the first few eigenvalues. The eigenvalue output from my code was a list of disordered eigenvalues. therefore, the more eigenvalues in my output, the more eigenvalues I had to sort in my list. So I had to devise a way to sort the real valued eigenvalues in order with increasing energy. To later plot only the lowest ones.

This was one of the reasons why my code was not the fastest. Another reason for my matrix method not being the most efficient was already explained in section 3.1.2.

4.4 Exceptional points

Energy quantization has a topological interpretation, when we extend the parameters of a Hamiltonian into the complex domain, we find that the energy eigenvalues are all branches of a multivalued function, they are analytical continuations of one another and can be continuously deformed into one another by varying the parameters. Energy levels are in a one to one correspondence with the sheets of a Riemann surface. From the narrow perspective of real variables this topological interpretation is invisible.

The behaviour of the eigenvalues of the Hamiltonian in equation (3.2) for the $\epsilon < 0$ region is a great demonstration of this. Note that there are ϵ values at which a minimum of two eigenvalues merge (the

order of the degeneracy depends on the number of coalescent eigenvalues at that point[1][6]), at $\epsilon = -1$ both Figure 1.3 on page 4, and my own renditions in sections 3.2.2 and 3.2.4 display an infinite-order exceptional point.

Energy levels follow closed paths in the complex energy plane, however if the closed path encircles an **exceptional point** (branch-point singularity), the energy levels exchange their identities because they are analytic continuations of one another[1][6]. This phenomenon is called level crossing. Interestingly, it is possible to vary the parameters of a Hamiltonian in laboratory experiments and thus to observe experimentally the effect of encircling exceptional points[6]. An example of this kind of experimental non-Hermitian degeneracy manipulation can be found in Gao et al (2015).

Finally, I have already explained that when a non-Hermitian Hamiltonian satisfies PT -symmetry (unbroken) the energy spectrum of the Hamiltonian in question has all real eigenvalues. Does this mean that the Hamiltonian I studied can be used to describe actual physics? The short answer is yes. The long answer requires the definition of a new non-trivial linear operator called the C operator. However, this topic was beyond my research at this time.

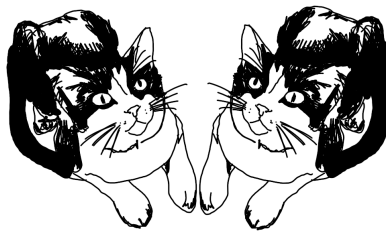
Chapter 5

Conclusion

Chapter 6

Acknowledgements

I want to thank my supervisors Jesper and Meera for giving me their time and for guiding me through the semester with great ideas and suggestions. I truly enjoyed all of the moments when we met to discuss physics and other topics. I also want to thank Daniel Price for giving me the opportunity to try out research in a formal setting by accepting my request to join this research unit and for being so attentive and responsive to my emails. Lastly, I want to thank my partner Chris for being an endless source of inspiration, helpful advice and for all our interesting rants and discussions.



Bibliography

- [1] Bender C M et al. *PT Symmetry*. WORLD SCIENTIFIC (EUROPE), 2019. [5](#), [1](#), [2](#), [4](#), [7](#), [8](#), [16](#), [17](#), [19](#)
- [2] Jones-Smith K A. Non-hermitian quantum mechanics, 2010. [2](#)
- [3] Bender C M. Making sense of non-hermitian hamiltonians. *Reports on Progress in Physics*, 70:947–1018, 2007. [3](#), [4](#), [7](#), [8](#)
- [4] Moiseyev N. *Non-Hermitian Quantum Mechanics*. Cambridge University Press, 2011. [5](#)
- [5] Press W H et al. *Numerical Recipes 3rd Edition: The Art of Scientific Computing*. Cambridge University Press, 3 edition, 2007. [6](#), [18](#)
- [6] Bender C M et al. Behavior of eigenvalues in a region of broken pt symmetry. *Physical Review A*, 95(5), 2017. [5](#), [7](#), [17](#), [19](#)
- [7] H Bauke. Calculating the hermite functions, Aug 2014. [10](#)
- [8] The SciPy community. numpy.argsort, Jan 2021. [11](#)
- [9] Sorrell M. Complex wkb analysis of a pt symmetric eigenvalue problem. *Journal of Physics A: Mathematical and Theoretical*, 40:10319–10335, 2007. [16](#)